NARROWBAND PROPAGATION STATISTICS OF AERONAUTICAL MOBILE-GROUND LINKS IN THE L- AND C-BANDS

Albert Smith, David W. Matolak, University of South Carolina, Columbia, SC
Robert J. Kerczewski, NASA Glenn Research Center, Cleveland, OH

Abstract

To provide for the safe integration of unmanned aircraft systems (UAS) into the National Airspace System (NAS), command and control (C2) links must be highly reliable. Hence, protected aviation spectrum is required to support such links for UAS that are integrated into controlled non-segregated airspace. For air-ground (i.e., non-satellite) links, protected aviation spectrum to support C2 links is available in the 960-1164 MHz (L) and 5030-5091 MHz (C) bands. The performance of any C2 system is critically dependent upon the characteristics of the air-ground (AG) channel. Therefore, as part of its UAS Integration in the NAS (UAS in the NAS) project, the U.S. National Aeronautics and Space Administration (NASA) performed a series of air-ground propagation flight tests to collect AG channel data for model development and analysis of potential C2 communications links capable of providing the required reliability. NASA's Glenn Research Center (GRC) conducted an extensive air-ground channel propagation measurement campaign (at altitude) for frequencies in the 960-977 MHz and 5030-5091 MHz ranges, for seven different terrain environments. The measurements were conducted in 2013, and produced the largest set of AG channel data ever gathered to date. This data was subsequently processed to develop models for the AG channel. The statistics collected enabled the derivation of channel model parameters for both narrowband and wideband channels. In order to make the propagation data widely available, the resulting narrowband statistics were processed and submitted to the International Telecommunications Union–Radiocommunication Sector (ITU-R) Study Group 3 Data Banks. Formats for data tables were developed, and tables of the aggregate narrowband propagation statistics for the seven ground site terrain environments were prepared, submitted to, and approved by, the ITU-R Study Group 3. This paper provides brief background on the measurement campaign, collection and processing of data, and development of the narrowband data tables. It further provides examples of the data and its use.

I. Introduction

Unmanned aircraft systems (UAS), also referred to as remotely piloted aircraft systems (RPAS), have emerged as the most significant vehicular advancement affecting airspace operations in decades. Although UAS developments were powered by military requirements, UAS have rapidly reached a level of technological advancement whereby many non-military uses have emerged. These non-military uses will often require operations in the same airspace as commercial and general aviation aircraft, especially for mid-size and large UAS.

Over the past several years, research into technologies needed to enable UAS operations in non-segregated airspace has been conducted with some urgency, as there is considerable pressure from the industry and public organizations to enable such integrated operations on a regular, routine basis rather than by exception. Among the key issues preventing such integration was the lack of developed standards for unmanned aircraft system (UAS) operations, as all previously developed standards and policies were based upon manned operations. Aircraft and system certification, sense and avoid techniques, air traffic management procedures, aircraft control human interfaces, and communications links are among the major elements of UAS integration under study.

As part of the US government's research efforts supporting integration of UAS into the NAS, NASA undertook the 5-year UAS Integration in the National Airspace System (NAS), or UAS in the NAS Project [1]. The project's key objectives included the following:

- Develop a body of evidence (including validated data, algorithms, analysis, and recommendations) to support key decision makers in establishing policy, procedures, standards and

regulations, enabling routine UAS access in the NAS.

• Provide methodologies for development of airworthiness requirements and data to support development of certification standards and regulatory guidance.

The UAS in the NAS Project's Communications Subproject addressed the need for robust, reliable C2 communications operating on radio-line-of-sight (LOS) AG links. To accomplish this, the Subproject focused on developing data and rationale to obtain and appropriately use frequency spectrum allocations for the safe and efficient operation of UAS in the NAS and enable the development and validation of national and international standards for C2 communications which could enable certification of UAS.

The International Civil Aviation Organization (ICAO) established a requirement that UAS C2 links using protected aviation spectrum were required for operations in non-segregated airspace. For UAS LOS C2 links, two candidate frequency bands were investigated: the 960-1164 MHz (L) and 5030-5091 MHz (C) bands. Both bands have international frequency allocations for Aeronautical Mobile (Route) Service (AM(R)S), as established by the International Telecommunications Union (ITU), through past World Radiocommunication Conferences. The AM(R)S allocation is the appropriate protected aviation band for UAS C2 AG communication links.

The UAS in the NAS Communications Subproject developed C2 prototype radios in both candidate bands [2]. Through flight testing of these radios, requirements and standards developed through RTCA Special Committee 228 were validated and final standards published as DO-362 in September 2016.

To support the prototype radio design, flight testing and standards development process, the Communications Subproject also sought to quantify characteristics of the air-ground (AG) propagation channel, to enable establishment of valid channel models to support communication link design and system performance analysis.

The AG propagation channel characterization was carried out through a series of AG channel flight measurement campaigns conducted primarily during 2013. The campaigns measured narrowband propagation data in the lower portion of the 960-1164 MHz band and both narrowband and wideband propagation data in the 5030-5091 MHz band. Campaigns were conducted for seven different terrain types. Extensive analysis of the resulting data enabled the establishment of the AG propagation channel characteristics for both bands [3]. Channel models based on these results have also been developed. [4].

A final activity, the focus of this paper, has been to prepare tables of the statistics derived from the AG channel measurements and make the data globally available. This has been accomplished by developing appropriate table formats for AG channel statistics for the ITU's Study Group 3 Data Banks, and populating these tables with statistics derived from the NASA AG channel flight measurement campaigns for each of the seven terrain types. For the narrowband data, the statistical tables for both frequency bands have been completed and accepted for inclusion in the Study Group 3 Data Banks as of the ITU Study Group 3 meetings of August, 2017. The derivation of the wideband statistics and completion of the wideband statistical tables are nearing completion at the time of this paper's preparation.

The following sections describe the AG channel measurement campaigns and processing of the resulting data. The development of the statistical results submitted to ITU Study Group 3 are then described, including examples of data tables. An explanation of the results and their significance and how they can be applied is provided, followed by concluding remarks.

II. AG Channel Measurements

A. Measurement Campaign Overview

Detailed descriptions of the measurements appear in [3] and [5], so here we only summarize the campaign. The seven ground site (GS) environments were as follows: over sea, over freshwater, hilly, mountainous, suburban, desert, and near-urban. The flight test aircraft was NASA GRC's S-3B Viking, depicted in Figure 1. The S-3B is a medium-sized piloted aircraft, accommodating two pilots and two research engineers, with the remaining space for test

equipment. The GS was designed to be portable: it was deployed via a transportable tower system on a trailer; see Figure 2. Power was provided to the GS by a 7 kW diesel generator. The GS contained a pneumatically-extendable mast, on which antennas were mounted. The mast is of adjustable height from 4 – 20 m. The remainder of the GS consists of a weatherproof cabinet for test equipment. For the AG channel measurements, this cabinet contained the channel measurement system transmitters, mast control, GPS receiver, and other associated electronics.

The AG channel measurement system is termed the channel sounder. This sounder was a custom design built specifically for application in these two frequency bands. The sounder consists of two transmitters and four receivers, and hence is denoted a single-input/multiple-output (SIMO) channel sounder. There is 1 transmitter (Tx) and 2 receivers (Rxs) in each band, i.e., a 1×2 system in each band. The sounder was developed by Berkeley Varitronics Systems, Inc. [6], according to specifications developed by the project principal investigator and NASA. The sounder operated simultaneously in the two frequency bands (L-band, 960-977 MHz, and C-band, 5030-5091 MHz). For all tests the two transmitted signal center frequencies were approximately 968 MHz and 5060 MHz.

Fig. 1. NASA GRC's-3B Viking aircraft.

Fig. 2. NASA GRC's transportable tower and GS system.

The two transmitter units employed direct-sequence spread spectrum (DS-SS) transmission. The C-band chip rate was 50 Mchips/sec, and the L-band chip rate was 5 Mchips/sec, providing signal bandwidths of approximately 50 MHz for C-band, and 5 MHz for L-band. The sounder's transmitted signals were filtered using root-raised cosine responses (rolloff ~0.3) for spectral containment. Hence the 50 MHz C-band signal had delay resolution approximately 20 ns, and the 5 MHz L-band signal had delay resolution approximately 200 ns. The DS-SS sequences were maximal-length sequences (*m*-sequences) of length 1023. At the aircraft, two antennas were available to connect to the two Rxs for each band: this amounts to four individual stepped-correlator DS-SS receivers. For all tests, the four receivers were on the aircraft and the two transmitters at the GS. The four Rx antennas were monopoles, hence nearly omnidirectional in azimuth, with approximate gains of 5 dB. These aircraft antennas were mounted on the bottom center of the S-3B fuselage in a rectangular pattern, with the same-band antennas located on opposite corners of the rectangle of size approximately 1.32 by 1.4 m.

The GS antennas were moderately directional: the C-band GS antenna gain is 6 dB and the L-band gain 5 dB. These antennas had elevation/azimuth beamwidths of approximately 35º/180º for C-band and 60º/120º for L-band. All antennas were vertically polarized, and for essentially all flight tests, the aircraft was within the GS antennas main beams. Detailed antenna patterns were reported in [7].

Transmitter output power for both bands was 10 watts (40 dBm). The C-band Tx also employed a 7 dB gain high power amplifier. Low noise amplifiers (LNAs) were also used at both receivers: a 30 dB LNA in C-band, and 15.5 dB LNA for L-band. Since the sounder required a minimum received signal-to-noise ratio (SNR) of approximately 10 dB, the C-band maximum range was limited to approximately 40 km, whereas the L-band range was nearly 200 km. Earth curvature restricted flight ranges to

approximately 40 km at the flight altitudes used in most tests. These altitudes ranged from approximately 400 m to 1.9 km.

Obviously, since flight tests are expensive and require significant coordination with air traffic control and other entities, only a representative set of GS locations was employed. These sites were selected for their local characteristics to represent a variety of conditions: hilly terrain, mountainous terrain, over-water (both freshwater and sea), suburban, desert, and near-urban. No channel measurements can cover every possible type of GS location, but as far as we are aware, these results are the most comprehensive set of results for the AG channel to date. The measurement campaign collected nearly 316 million channel impulse responses (CIRs) in total, for the seven different GS settings. Additional details regarding the characteristics of the GS environments are provided in [3]. In Figure 3 we show several example flight tracks (FTs, using Google Maps®) in the hilly and suburban setting of Latrobe, PA (top), and a photograph of the Latrobe township (bottom), near the GS.

Flying in controlled airspace naturally constrains the flight paths we could follow. Our flight path shapes were either straight, both toward and away from the GS, or oval-shaped, as illustrated in Figure 3. The straight flight paths enable quantification of channel characteristics versus distance, and the oval flight paths varied aircraft antenna orientation. Flight test planning had to account for limits on minimum altitude, proximity to populated areas, flying times, and flight velocities. Although not significant for propagation at our frequencies, weather was clear during all flights. The S-3B Viking aircraft also had limitations on its minimum flight velocity. All FTs were flown at a nearly constant altitude, with link ranges for measurements ranging from 1-40 km. Flight velocities ranged from approximately 75 m/s to 100 m/s.

B. Data Processing

The channel sounder measured CIRs in the form of amplitudes and phases of all multipath components (MPCs). For delay domain channel statistics these are converted to power delay profiles (PDPs). The channel measurement, or "snapshot," rate was approximately 3000 PDPs/second. The

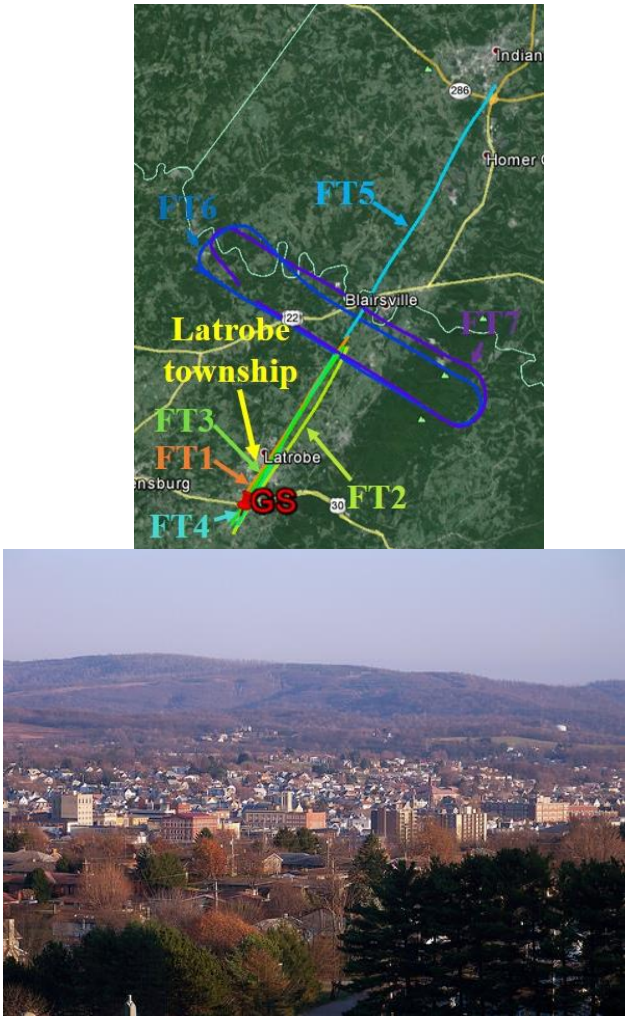

Figure 3. Google Maps® views of flight tracks (FTs) taken in suburban setting in Latrobe, PA (top), and photo of Latrobe township (bottom).

PDP is essentially the power output at time t vs. delay τ, when an impulse is input at time t-τ. The GS and aircraft also carried GPS receivers that provided position information for each PDP. From these CIRs, several channel characteristics were estimated: attenuation or propagation path loss, delay dispersion (delay spread), Doppler effects, small-scale amplitude fading characteristics, and correlations among the signals received on the different antennas and in the two frequency bands.

The DS-SS signal employs a pulse-compression CIR estimation technique, via correlating the received sampled signal with a local copy of the transmitted *m*-sequence. Two thresholds were applied to the received CIRs: the first threshold was 25 dB below the largest received signal component,

and the second was an absolute noise threshold. All sounder correlator outputs below these thresholds were removed before subsequent processing for channel parameter estimates, as their low power would contribute little. As expected, the largest received signal component was the line-of-sight (LOS) component, which was present for all flight tests. The absolute noise threshold was employed to remove (with probability approximately 0.9995) external noise that was caused by other aircraft electronic equipment; see [5] for analysis. The two thresholds were applied after the despreading of the DS-SS signal, at the Rx correlator outputs. We also applied additional time-domain processing of PDPs to identify and remove the rare noise spikes that remained after the two thresholds.

From the measured data, the following AG channel characteristics were estimated:

1. propagation path loss, or attenuation (dB);

2. stationarity distance (m);

3. Ricean K-factor (dB);

4. correlation coefficients (dimensionless);

5. airframe shadowing depths (dB) and durations (sec);

6. multipath component statistics.

The computational methods used for parameter estimation are described in [3] and [8]-[10]. Path loss is computed via link budget equations. Stationarity distance (SD) is a relatively new characteristic of study in the propagation and channel modeling community, and it can be computed using multiple methods. Roughly speaking, SD is the spatial extent over which the channel statistics are approximately constant. Our SD estimates used the methods of [11] and [12]. The Ricean K-factor was computed using two methods, a moment-based method [13] and the maximum-likelihood method [14]. Both methods yielded essentially identical K-factor estimates. Correlation coefficients were computed for the LOS component signals on all four antennas. Hence both same-frequency (C-C, and L-L) spatial correlations and different-frequency (C-L) spatial correlations were computed. All correlations and Ricean K-factors were computed over the SD of approximately 15 m. All these factors are relevant to the narrowband statistics we present in the next section.

Airframe shadowing is the attenuation caused by blockage of the LOS component by the aircraft itself. These shadowing events were intentionally induced by banking turns in the oval-shaped FTs. Although shadowing could be incorporated into narrowband attenuation statistics, we have quantified it separately. Specifically, such shadowing was computed as the attenuation relative to the best-fit log-distance path loss model. See [10] for specifics.

The MPC statistics are most relevant for the wideband statistics, but for completeness we provide a short description here. The MPC statistics we computed are the amplitudes relative to the LOS component (in dB), the delays relative to the LOS component delay (in sec), the MPC durations or "lifetimes" (in m), and the MPC probabilities of occurrence. Wideband statistical tapped-delay line models were developed for the AG channel via a detailed analytical two-ray model, accounting for the LOS component and primary earth surface reflection, combined with the MPC statistics. The resulting AG channel models are "quasi-deterministic," or hybrid geometry-based (deterministic) and empirical statistical models.

III. Narrowband Channel Statistical Results

A. Example Statistics

To describe environments statistically, the ITU defines fade depth *A* as the attenuation in dB relative to the line-of-sight (LOS) component. Statistics of *A* are often specified for a given percentage of time. In equation form *A* is

$$A = L_{fs} - L_{meas}\ , \qquad (1)$$

where L_{fs} is free-space path loss and L_{meas} is the measured path loss (both in dB). The free-space loss is $20log(4\pi d/\lambda)$ dB, with d the link distance and λ wavelength. When the measured path loss is larger than free-space path loss (*A* is negative), the event is called a fade. The case when *A* is larger than zero indicates that there is constructive interference and in general is uncommon. This up-fade, or decreased measured path loss, can be attributed to strong reflections in the environment.

Figure 4 plots two representative examples of narrowband statistical results for *A* and its occurrence in time. This is a direct plot of what the

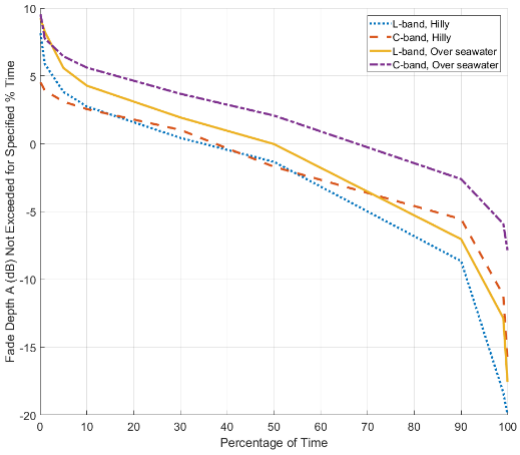

Figure 4. Fade depths not exceeded for given percentage of time for L-band and C-band over hilly and over seawater environments.

ITU narrowband data tables contain, here for both frequency bands, for two distinct GS environments.

It can be easily seen in Figure 4, that in general the over seawater environment gives a larger value for *A* than the hilly environment. This means that the over seawater case had much smaller measured pathloss (relative to free space) than did the hilly environment. It can also be seen that for a large portion of given percentages of time the over seawater environment has a fade depth larger than 0 dB. This means that the measured pathloss is *less* than the free-space pathloss, indicating that there is constructive interference: this is a well-known effect seen with 2-ray channels, which the over water surface environments well approximate.

Plots like those of Figure 4 that are based directly upon the tabulated ITU data could be viewed as somewhat difficult to interpret. Hence to provide an alternate, potentially clearer version, we have re-plotted some of these results as follows. We describe fade depths in *positive* numbers, and define a new fade variable *F* as,

$$F = L_{meas} - L_{fs} = -A. \qquad (2)$$

Under this convention, when F is a positive number, there is a fade—a reduction in signal strength relative to free-space—of *F* dB. We also revise the temporal scale to express fades in terms of fraction of time instead of percentages, and exchange the abscissa and ordinates. Re-plotting Figure 4 in this manner yields Figure 5, which is of the form of a conventional cumulative distribution function (cdf).

For an example interpretation, the C-band over sea result shows that for a fraction of time approximately 0.7, path loss was less than that of free space ($F<0$), whereas this fraction of time with $F<0$ for the L-band hilly case was only 0.4. For fades *greater* than a given value we subtract the cdf value, e.g., in the L-band hilly case, fades deeper than approximately 10 dB ($F>10$) occurred for fraction of time 1-0.91=0.09.

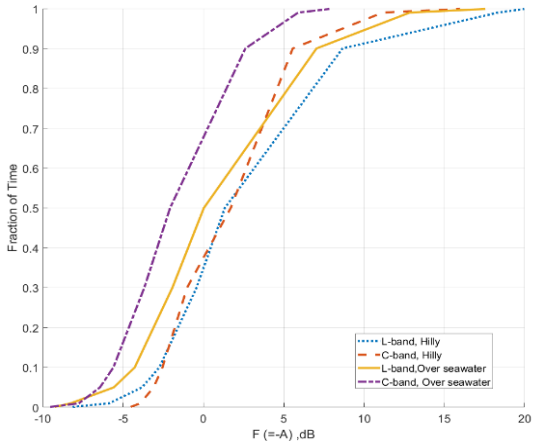

Figure 5. CDFs for L-band and C-band over hilly and over seawater environments.

The other information the ITU uses to characterize narrowband fading environments is the length of fade durations for a given percentage of time, at a selected fade level. An example table is provided in plot form in Figure 6 for the C-band frequency in a desert environment. The ITU defines these fade durations in seconds.

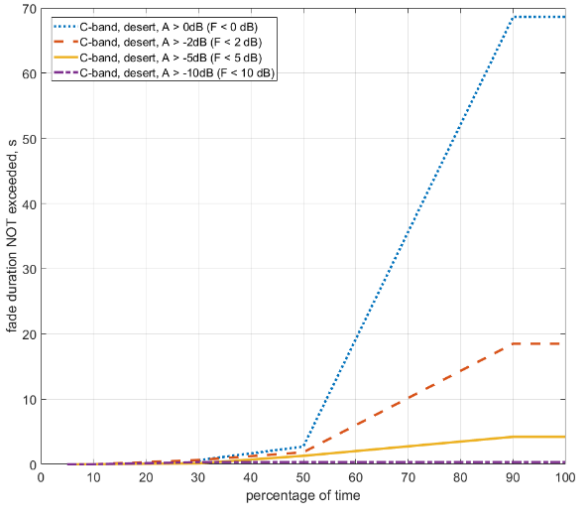

Figure 6. Fade durations (s) not exceeded for given percentage of time.

For this case, for 50% of the time, fades of up to 5 dB (F< 5 dB) last approximately 1 second or less. For 50% of the time, fades of up to 0 dB (F<0 dB) last for approximately 3 seconds or less. For 90% of the time, fades of up to 5 dB below LOS last for less than approximately 5 seconds. The general trend is as expected; as larger percentages of time increase the maximum fade duration value *not* exceeded. In these AG flight tests the specific flight tracks for which we computed statistics were straight paths. Hence the temporal fades correspond to spatial fade distributions. In fact, representing fades as having spatial extents is more useful because it removes the dependence on specific flight velocities associated with plots of the form of Figure 6. Fade durations in seconds are converted to fade durations in meters based on the known velocity of the aircraft. This allows the use of these data tables for any aircraft traveling at an arbitrary velocity. Figure 7 shows Figure 6 re-plotted in this manner.

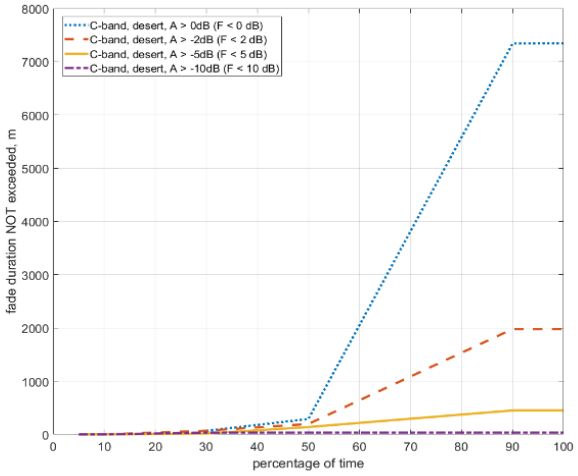

Figure 7. Fade durations (m) not exceeded for given percentage of time.

In the spatial representation of Figure 7, for 50% of the time, fades of up to 5 dB (F< 5 dB) last for less than approximately 150 meters. For 90% of the time, fades of up to 5 dB (F< 5 dB) last for less than approximately 500 meters. For 90% of the time, fades of up to 2 dB below LOS last for less than approximately 2000 meters.

Associated with all the narrowband ITU data tables is a set of descriptive data that enables readers to understand the origin of the data. This data describes conditions of the flight tests, and hence can be used by readers to assess applicability for their own conditions of interest. Table 1 provides an

Table 1. Testing conditions for narrowband statistics of aeronautical mobile-ground links for 5030-5091 MHz (C-band) over sea.

Frequency f (GHz)	5060MHz
Polarization (L/C)	Linear (vertical)
Polarization tilt angle φ_p (degrees)	NA
Signal source	
Ground Station latitude (–90…+90) (degrees)	34.1770°
Ground Station longitude (–90…+90) (degrees)	-119.2354°
TX antenna gain towards mobile (dBi)	6
TX 3 dB beamwidth θ_r (degrees, azimuth)	180
TX 3 dB beamwidth θ_r (degrees, elevation)	35
Local ground site characteristics (5)	70
TX antenna height ag h_t (m)	23.4696m
Aeronautical mobile station	
RX Aircraft Type	Lockheed S-3B Viking
RX country(1)	USA
RX Path Type (linear, oval, etc.)(2)	Linear
RX start latitude (–90…+90) (degrees)	34.2456°
RX start longitude (0..360) (degrees) E	240.516°E
RX end latitude (–90…+90) (degrees)	34.19475°
RX end longitude (0…360) (degrees) E	240.748°E
RX average altitude amsl h_{gr} (m)	797.619m
RX antenna type	quarter-wavelength monopole
RX 3 dB beamwidth θ_r (degrees, azimuth)	NA
RX antenna gain (dBi)	5
RX multipath reduction? (Y/N)	N
RX dynamic range (dB)	60
RX integration time (s)	variable
Data sampling interval (s)	0.000333
Data resolution (dB)	0.5
Measurement: Experiment No.	Aggregate
Start date (yyyy.mm.dd)	2013.06.11
End date (yyyy.mm.dd)	2013.06.11
Duration d (days) (3)	6424.91sec=.07436d
Average elevation angle (degrees)	3.1589 °
Range of elevation angles (degrees)	0.69172° to 20.5002°
Average velocity of aircraft (m/s)	90.7912m/s
Environment	
Over Sea	
Weather conditions(4)	
Ground temperature range at TX	
Land mobile terrain type(5)	70
Land mobile building type(5)	70
Land mobile vegetation type(5)	70
Land mobile surface shape(6)	overwater
Sea state	WMO Sea State Code 2
80% CDF of basic transmission loss, L80 (dB)	137.57
90% CDF of basic transmission loss, L90 (dB)	138.82

example of this descriptive text used in the ITU narrowband statistics tables.

B. Summary of Statistical Results

It is recommended that fade depth information from our narrowband results be expressed using *F*, as defined in (2); this facilitates utilization of the CDF presentation format. Similarly, fade durations are best expressed in meters, to remove dependence on our specific flight velocities.

Obviously, these results can be readily used in standard link budget equations, e.g.,

$$P_r = P_t + G_t + G_r - L \quad (3)$$

where P_r is the received power in dB units (dBm or dBW, typically), P_t is the transmitted power in dB units, G_t is the gain of the transmitter antenna in dB, G_r is the receiver antenna gain in dB, and L is the attenuation in the channel in dB, defined as

$$L = L_{fs} + F \quad (4)$$

where L_{fs} is the free-space pathloss and F is the fade depth as described in Section III. By selecting the fraction of time and environment type, estimates can be made for how much additional power relative to free-space will be needed to maintain a given link. As an example, for a hilly environment the condition of not being in a fade for half of the time (50% of the time), an additional 1.70 dB is needed for C-band and 1.33 dB is needed for L-band. To provide a high degree of confidence (99% of the time), much more additional gain is required. For the same hilly environment, C-band requires an additional 11.16 dB and L-band requires an additional 18.34 dB. Additional values for *F* are provided in Tables 2 and 3 for C-band and L-band environments.

One can use these tables as described to estimate link margins required to achieve desired fraction of time reliabilities. Of course such fractions of time are not the only statistics of importance, especially at these particular fade depths specified by the ITU (as in Figure 6). For example, maximum fade depths are not readily apparent, and even though rare, may be important for very high reliability UAS links. Thus although the over-water L-band channel appears fairly benign, 2-ray fades exceeding 18 dB were measured in that case. The models in [3] and [8]-[10] could be used to augment such analyses conducted with the narrowband ITU data tables.

Table 2. C-band environment fade depths, *F* in dB.

Environment	1% of time Fade depth, F	50% of time Fade depth, F	99% of time Fade depth, F
Over Seawater	-7.76	-2.08	5.90
Over Freshwater	-6.99	-1.14	7.03
Hilly	-3.93	1.70	11.16
Mountainous	-5.17	0.58	12.29
Suburban	-6.97	-0.42	9.61
Desert	-8.71	-2.24	5.54
Near-Urban	-6.82	-0.37	6.18

Table 3. L-band environment fade depths, *F* in dB.

Environment	1% of time Fade depth, F	50% of time Fade depth, F	99% of time Fade depth, F
Over Seawater	-8.27	0.02	12.85
Over Freshwater	-5.11	2.96	12.44
Hilly	-5.89	1.33	18.34
Mountainous	-5.70	2.93	13.12
Suburban	-5.84	2.02	10.80
Desert	-6.20	0.84	11.05
Near-Urban	-3.47	1.85	9.17

For both C-band and L-band frequencies, the environments with the deepest fades (for the majority of time) are the hilly and mountainous terrains. The hilly environment included the largest buildings that yielded strong multipath reflections. For C-band frequencies, the over seawater and over freshwater conditions produce small fading depths; these surfaces are rough at this frequency, and of course fewer multipath components are present in the over-water settings. The over water cases give up-fades (decrease in measured pathloss relative to

free-space) values that are consistent with a 2-ray channel, up to approximately 6 dB.

IV. Conclusion

In this paper we described the UAS in the NAS project and its importance in collecting data useful for the evaluation and design of high-reliability command and control links for UAS. A large amount of this data was AG flight test data, and this enabled us to gather statistics on fade depths relative to free-space path loss in these line-of-sight links. This data was organized and presented to the ITU for inclusion in their data banks, and hence the narrowband fading statistics can be used by the community for AG link analysis and design.

References

[1] R. J. Kerczewski, J. H. Griner, "Control and Non-Payload Communications Links for Integrated Unmanned Aircraft Operations," *18th Ka and Broadband Communications Conference/30th AIAA ICSSC Joint Conference*, Ottawa, Canada, September 2012.

[2] K. A. Shalkhauser, J. A, Ishac, D. C. Iannicca, S. C. Bretmersky, A. E. Smith, "Control and Non-Payload Communications (CNPC) Prototype Radio Validation Flight Test Report," NASA Technical Memorandum 2017-219379, July 2017.

[3] D. W. Matolak, R. Sun, "Air-Ground Channel Characterization for Unmanned Aircraft Systems—Part I: Methods, Measurements, and Results for Over-water Settings," *IEEE Trans. Veh. Tech.*, vol. 66, no. 1, pp. 26-44, Jan. 2017.

[4] D. W. Matolak, "AG Channel Measurement, Modeling, and Communication Link Results for UAS," (Report #10) Final Report for NASA Grant #NNX12AR56G, 27 October 2016.

[5] D. W. Matolak, R. Sun, "AG Channel Measurement & Modeling Results for Over-Sea Conditions," (Report #6) NASA Grant #NNX12AR56G, 3 December 2013.

[6] Berkeley Varitronics Systems, website www.bvsystems.com, 6 March 2018.

[7] R. Sun, D. W. Matolak, "Over-Harbor Channel Modeling with Directional Ground Station Antennas for the Air-Ground Channel," *2014 Military Communications Conference (MILCOM 2014)*, pp. 1-6, Baltimore, MD, 6-8 Oct. 2014.

[8] R. Sun, D. W. Matolak, "Air-Ground Channel Characterization for Unmanned Aircraft Systems—Part II: Hilly & Mountainous Settings," vol. 66, no. 3, pp. 1913-1925, March 2017.

[9] D. W. Matolak, R. Sun, "Air-Ground Channel Characterization for Unmanned Aircraft Systems—Part III: The Suburban and Near-Urban Environments," *IEEE Trans. Veh. Tech.*, vol. 66, no. 8, pp. 6607-6618, August 2017.

[10] D. W. Matolak, R. Sun, W. Rayess, "Air-Ground Channel Characterization for Unmanned Aircraft Systems—Part IV: Airframe Shadowing," *IEEE Trans. Veh. Tech.*, vol. 66, no. 9, pp. 7643-7652, September 2017.

[11] A. Gehring, M. Steinbauer, I. Gaspard, M. Grigat, "Empirical Channel Stationarity in Urban Environments," *4th European Personal & Mobile Comm. Conf. (EPMCC 2001)*, Vienna, Austria, 20-22 February 2001.

[12] O. Renaudin, V-M Kolmonen, P. Vainikainen, C. Oestges, "Non-Stationary Narrowband MIMO Inter-Vehicle Channel Characterization in the 5 GHz Band," *IEEE Trans. Veh. Tech.*, vol. 59, no. 4, pp. 2007-2015, May 2010.

[13] L. J. Greenstein, S. S. Ghassemzadeh, V. Erceg, D. G. Michelson, "Ricean K-Factors in Narrow-Band Fixed Wireless Channels: Theory, Experiments, and Statistical Models," *IEEE Trans. Vehicular Tech.*, vol. 58, no. 8, pp. 4000-4012, Oct. 2009.

[14] C. Tepedelenlioglu, A. Abdi, G. B. Giannakis, "The Ricean K factor: estimation and performance analysis," *IEEE Trans. Wireless Comm.*, vol. 2, no. 4, pp. 799-810, July 2003

Acknowledgements

The authors would like to thank the UAS in the NAS team at NASA GRC for their extensive work in collecting the flight test data.